EXPLORATION OF CASSON FLUID-FLOW ALONG EXPONENTIAL HEAT SOURCE IN A THERMALLY STRATIFIED POROUS MEDIA

by

Priyanka AGRAWAL[a], Praveen Kumar DADHEECH[a], Ram Niwas JAT[a], Dumitru BALEANU[b,c,d], and Sunil Dutt PUROHIT[e*]

[a] Department of Mathematics, University of Rajasthan, Jaipur, India
[b] Department of Mathematics, Cankaya University, Ankara, Turkey
[c] Institute of Space Sciences, Magurele-Bucharest, Romania
[d] Lebanese American University, Beirut, Lebanon
[e] Departmetn of HEAS (Mathematics), Rajasthan Technical University, Kota, India

Original scientific paper
https://doi.org/10.2298/TSCI23S1029A

Objective of the present investigation is intended to study the MHD Casson fluids flow through an exponentially stretching surface. This free convective flow is investigated in thermally stratified porous medium. Also viscosity along with thermal conductivity is varying with temperature. With the exponential decay for the internal heat generation in the region and buoyancy force, the natural-convection is induced. Then the transformed set of equations of the flow after applying suitable similarity solutions were encountered by Shooting Technique in conjunction with the fourth ordered Runge-Kutta method. Outputs illustrates that with increased viscosity parameter an increasing velocity profile is noticed but a decrement is observed for temperature field in entire domain and near the wall for temperature gradient profile. Also with increased Casson fluids parameter decreasing velocity profile is noticed but an increment is observed for temperature field in entire domain and for temperature gradient profile near the wall.

Key words: *Casson fluid, porous media, variable thermal conductivity, variable viscosity, thermal stratification, MHD*

Introduction

Investigation on the flow of the laminar boundary-layers considering the non-Newtonian fluids over stretching/shrinking surfaces with porous media has important applications in the technology of chemical science and materials science. The analysis of heat transmission in laminar flows via expanding surfaces has attracted substantial interest because of its numerous practical applications, such as pipe manufacturing, drawing of plastic films, and treatments related to blood flow, *etc.* Initially With the stretching sheets, Crane [1] investigated the precise analytical expressions of boundary-layer flow. Earlier, it was assumed that the position from the source varied linearly with the velocity of the surface, but Gupta and Gupta [2] demonstrated that this is not the case for the surfaces that only stretches linearly. Afterwards, Kumaran and Ramanaiah [3] considered quadratic relation between the stretching sheet and distance. Elbashbeshy [4] investigated heat transfer in boundary-layered flows by considering exponential relation between the stretching sheet and distance from surface along with heat sink. Jat *et*

* Corresponding author, e-mail: sunil_a_purohit@yahoo.com

al. [5] investigated heat transport of radiative MHD flow of Caisson fluid through a moving permeable plate. Al-Odat *et al.* [6] have also studied MHD flow by considering, exponentially stretching surface.

The MHD is a powerful technique for regulating heat transfer. The scientists investigated the influence of an imposed charismatic field in which the sheet expands exponentially in a variety of states. Watanabe *et al.* [7] published a report of MHD free convection flow. Crepeau and Clarksean [8] investigated natural convective flow with exponential decay of internal heat generation. The findings indicate that the internal heat generation impact must be addressed in various applications, such as, nuclear reactors, electronic cooling, thermal insulations, and so on. In several cases, a noticeable temperature gap between the surfaces and the surrounding fluids may exist. This generates a need of heat sources that depends on temperature, which can have a significant impact on heat transfer performance, reported by Dessie and Kishan [9].

When water bodies are characterized by the layers of different temperatures then this phenomenon is called thermal stratification. This idea isolates water bodies into three layers named epilimnion, metalimnion and hypolimnion according to their temperature. Most elevated and hottest layer is named as epilimnion, whereas metalimnion is the intermediate layer and the layer close to the base, is hypolimnion. As of late, numerous analysts have detailed free convective flows over surfaces/plates implanted in thermally defined mediums, because of its practical applications. Animasaun [10] analyzed the impact of thermally stratified nanofluids on magnetic field with porosity and free convection and concluded that with increased thermal stratification parameter rate of heat transfer increases. Mabood *et al.* [11] analyzed the MHD Oldroyd-B fluids flow through expending sheet considering heat generation/absorption and thermal stratification. Tharapatla *et al.* [12] investigated effects of non-Newtonian fluids flow considering thermal stratification along with porosity.

The novelty of this investigation intended to scrutinize the transportation of heat of MHD Casson fluids flow through an exponentially stretched surface within a thermally stratified porous media considering variable thermal conductivity and viscosity. Graphical analysis presented of the velocity, temperature and temperature gradient fields in terms of several non-dimensional parameters. Comparison with previous studies is also presented.

Mathematical model

In this investigation electrically conducted fluids flow in 2-D, is considered. Viscous incompressible and study flow is studied. With uniformly imposed magnetic strength over exponential stretching sheet within a pore-filled medium investigated. In comparison of induced magnetic force, the induced magnetic force is presumed to be negligible. Taking these assumptions, the equation of the governing convective flows of the nanofluid is described:

$$\frac{\partial u}{\partial x}+\frac{\partial v}{\partial y}=0 \tag{1}$$

$$u\frac{\partial u}{\partial x}+v\frac{\partial u}{\partial y}=\frac{\partial}{\partial y}\left(\upsilon\frac{\partial u}{\partial y}\right)-\frac{\sigma\left[B(x)\right]^2}{\rho}u-\frac{\upsilon}{k}u+\mathrm{g}\beta^{+}(T-T_{\infty}) \tag{2}$$

$$u\frac{\partial T}{\partial x}+v\frac{\partial T}{\partial y}=\frac{\kappa}{\rho C_p}\frac{\partial^2 T}{\partial y^2}-\frac{1}{\rho C_p}\frac{\partial q_r}{\partial y}+\frac{Q_0}{\rho C_p}(T_w-T_0)e^{-\eta y\sqrt{\frac{U_0}{2\upsilon L}}e^{x/2L}} \tag{3}$$

The notations of velocities towards x-axis and y-axis are u and v, accordingly as represented in fig. 1, $\upsilon = (\mu/\rho)$ is the kinematic viscosity, ρ – the density, viscosity coefficient is μ, $k = k_0 e^{-x/L}$ non-uniform permeability of the media here k_0 is a the constant, d$B(x)$ is the magnetic field and given by $B(x) = B_0 e^{x/2L}$, where L represent the reference length and B_0 is the constant.

The plate's surface is considered very elastic and it stretches vertically along x-axis as velocity increase:

$$u = u_w(x) = U_0 e^{x/L},\ v_w(x) = v_0 e^{x/L},\ T_w(x) = T_0 + b e^{x/2L},\ T_\infty(x) = T_0 + c e^{x/2L} \tag{4}$$

where U_0 is the constant. Exponential velocity, $U_0 e^{-x/L}$, is considered only for $x \ll L$. When $x \geq L$, because in this case exponential velocity becomes very high also $c \geq 0$ and $b > 0$ are constants.

For the aforementioned problem the appropriate conditions of boundary provided through:

$$\begin{gathered} u = U_w(x),\ v = -V_w(x),\ T = T_w \ \text{ at } \ y = 0 \\ u \to 0,\ T = T_\infty \ \text{ as } \ y \to \infty \end{gathered} \tag{5}$$

where V_w is the velocity of injection ($V_w > 0$) and suction ($V_w < 0$), T_∞ – the ambient temperature, T_w – the temperature at surface, and T_0 – the reference temperature. According to the concept of viscosity ($\tau = \mu(\partial u/\partial y)|_{y=0}$), also with rheological equations of isotropic Casson fluids flow is defined [13]:

$$\tau_{ij} = \left(\mu_b + \frac{P_y}{\sqrt{2\pi}}\right)2e_{ij} \ \text{ when } \ \pi > \pi_c \ \text{ and } \ \tau_{ij} = \left(\mu_b + \frac{P_y}{\sqrt{2\pi_c}}\right)2e_{ij} \ \text{ when } \ \pi < \pi_c \tag{6}$$

where P_y corresponds to yield stress of fluid:

$$P_y = \frac{\mu_b\sqrt{2\pi}}{\beta} \tag{7}$$

where μ_b is the plastic dynamic viscosity, π – the component wise products of deformation rates by itself, that is $\pi = e_{ij}e_{ij}$, where e_{ij} corresponds to $(i, j)^{\text{th}}$ components of the deformation rate also π_c denotes critical number for non-Newtonian modulation. For Casson fluids (non-Newtonian) flow, the value of $\pi > \pi_c$, it can be defined:

$$\mu = \mu_b + \frac{P_y}{\sqrt{2\pi}} \tag{8}$$

Using eq. (5) in previous equation, Casson fluid's kinematic viscosity has now been reduced:

$$\mu = \mu_b\left(1 + \frac{1}{\beta}\right) \tag{9}$$

The Rosseland approximation needs optically dense medium and radiations that travels just a small distance before scattering or absorption. Radiative heat transfer is brought into consideration since we are investigating a case where heat is radiated within an optically thick Casson fluid before it is dispersed. Casson fluid is optically thick in this study, therefore, heat radiation only goes a short distance before being scattered or absorbed. To account for the radiative heat flux in non-Newtonian fluids, the Rosseland approximation is used, which is a refinement of the radiative transfer equation (RTE) for optically thick media [14, 15] is given:

$$q_r = -\frac{4\sigma^*}{3k^*}\frac{\partial T^4}{\partial y} \tag{10}$$

where σ^* is the constant of Stefan-Boltzmann with k^* – the coefficient of absorption.

To solve the mathematical model, the similarity transformations are being used [10, 16]:

$$u = \frac{\partial \psi}{\partial y},\ v = -\frac{\partial \psi}{\partial x} \tag{11}$$

$$\psi = \sqrt{2\upsilon L U_0} f(\eta) e^{x/2L} \text{ and } \eta = y\sqrt{\frac{U_0}{2\upsilon L}} e^{x/2L} \tag{12}$$

where $\psi(x, y)$ defined as stream function and following physical quantities are defined as [17]:

$$\theta(\eta) = \frac{T - T_\infty}{T_w - T_\infty},\ \mu_b(T) = \mu_b^* + a\mu_b^*(T_w - T),\ \kappa(T) = \kappa^* + \mathrm{d}\kappa^*(T - T_\infty) \tag{13}$$

where μ_b^* is the constant viscosity away from wall. Following the foregoing transformations, eqs. (2) and (3) are turned in non-linear ODE:

$$\left(1+\frac{1}{\beta}\right)\left(1+\zeta-\zeta\theta-\zeta S_t\right) f''' - \zeta\left(1+\frac{1}{\beta}\right)\theta' f'' - K\left(1+\frac{1}{\beta}\right)\left(1+\zeta-\zeta\theta-\zeta S_t\right) f' + \\ + ff'' - 2f'^2 - Mf' + G_{rm}\theta\zeta = 0 \tag{14}$$

$$\left(1+\varepsilon\theta+\frac{4}{3N}\right)\theta'' + \varepsilon\theta'^2 + \mathrm{Pr}\left[f\theta' - S_t f' - \theta f' + q_1 e^{-n\eta}\right] = 0 \tag{15}$$

With boundary conditions:

$$\eta = 0,\ f(\eta) = S,\ f'(\eta) = 1,\ \theta(\eta) = 1 - S_t;\ \eta \to \infty,\ f(\eta) \to 0,\ \theta(\eta) \to 0 \tag{16}$$

Also the non-dimensional parameters of physical importance are obtained:

$$K = \frac{2L\upsilon}{k_0 U_0} \text{ permeability parameter, } M = \frac{2\sigma B_0^2 L}{\rho U_0} \text{ magnetic parameter,}$$

$$\mathrm{Gr}_m = \frac{2g\beta^+ L}{bU_0^2 e^{2x/L}} \text{ local modified Grashof related parameter, } S_t = \frac{c}{b} \text{ stratification parameter,}$$

$$N = \frac{k^*\kappa^*}{4\sigma^* T_\infty^3} \text{ thermal radiation parameter, } \zeta = a\left(T_w - T_0\right) \text{ plastic dynamic viscosity parameter,}$$

$$\varepsilon = d\left(T_w - T_0\right) \text{ thermal conductivity parameter, } \mathrm{Pr} = \frac{\mu C_p}{\kappa} \text{ Prandtl number, and}$$

$$q_1 = \frac{2LQ_0}{U_0 \rho C_p e^{x/L}} \text{ heat source parameter}$$

Results and discussion

The results of the computational approach are achieved for a number of physical non-dimensional parameters that are depicted by graphs. The outcomes are used to show how different physical parameters affect temperature profiles $\theta(\eta)$, velocity profiles $f'(\eta)$, and temperature gradient profiles $\theta'(\eta)$.

Figure 1 depicts the impact of ξ on $f'(\eta)$. With increased ξ an increasing velocity profile is noticed. Since plastic dynamic viscosity of Casson fluid is considered as constant and when

there is plastic dynamic viscosity is variable then very small magnitude of velocity is observed at entire boundary-layer. Increasing temperature differences reduces intermolecular force of fluid and reduces the viscosity strength, significantly. Hence momentum boundary-layers increases as with this effect. The effect of ξ on $\theta(\eta)$ is depicted by fig. 2. The graph illustrates the significant impact of the strength of inner heat generation in the region. The temperature field is parabolic with the pick somewhat away from the surface are noticed decreasing for increasing ξ. With increasing ξ, thermal boundary-layer thickness increases, this leads to decreased $\theta(\eta)$, that results to slower velocity of the fluid. Impact of ξ on $\theta(\eta)$ is depicted by fig. 3. Heat transfer rate depends on the magnitude of $\theta'(\eta)$ in certain direction. Near the wall $\theta'(\eta)$ decreases with increased ξ and after a crossover point reverse effect is observed.

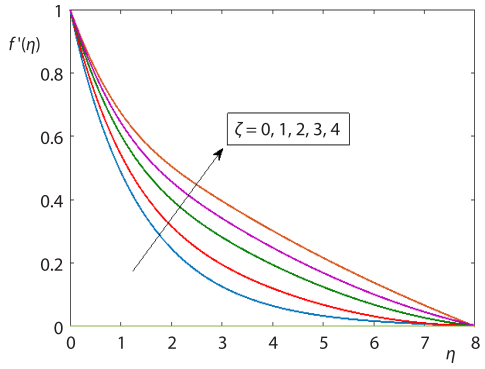

Figure 1. Velocity distribution for ξ

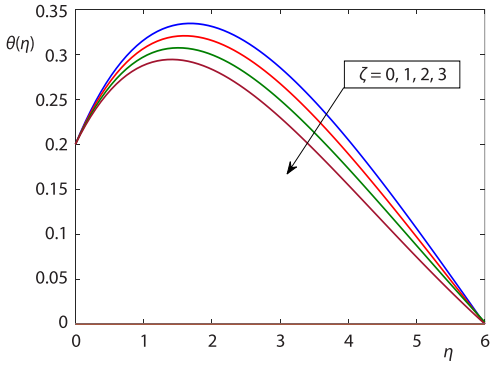

Figure 2. Temperature distribution for ξ

Figure 4 depicts the impact of S_t on $f'(\eta)$. It has been noted that with increased S_t a decrement is seen in $f'(\eta)$. This outcome may be followed to the way that, with increased S_t, the hotness of surface inside thermally stratified medium reaches from epilimnion hypolimnion. Figure 5 depicts the impact of S_t on $\theta(\eta)$. It has been noted that by increased S_t a decrement is seen in $\theta(\eta)$. Since with increased S_t, wall temperature decreases. The reverse effect is observed in temperature gradient profile $\theta'(\eta)$ for S_t as depicted in fig. 6. With increased S_t an increased $\theta'(\eta)$ is noticed.

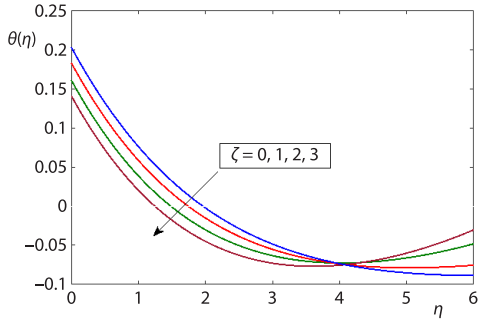

Figure 3. Temperature gradient distribution for ξ

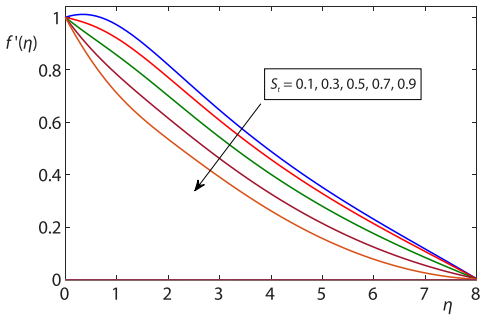

Figure 4. Velocity distribution for S_t

Figure 7 illustrates the impact of β parameter, on $f'(\eta)$. Here two cases are discussed, in first case ($\xi = 0$ and $S_t = 0.8$ hypolimnion layer) velocity profile decreases with increasing values of β. With high viscosity of Casson fluid, both cases cannot generate enough heat that can crack molecules that can cover up viscosity, therefore, decreased velocity is noticed. In sec-

ond case ($\xi = 4$ and $S_t = 0$ epilimnion layer) decreased velocity profile is noticed for increased β near the wall and reverse effect is notice after a crossover point for $\beta \to \infty$ (*i.e.* non-Newtonian to Newtonian fluid). For this case, the effect is clearly evident, the hotness of exponentially extending surface rises, and additional heat produces thus the molecular bonds are broken with the effect of ξ. These two cases are also discussed with temperature profile for the parameter β in fig. 8. With increased β an increment is noticed for $\theta(\eta)$ in first case (*i.e.* $\xi = 0$ and $S_t = 0.8$) and opposite effect is observed in second case (*i.e.* $\xi = 4$ and $S_t = 0$). As depicted in fig. 9 the temperature gradient is noticed to increases alongside the wall and decreases beyond the cross-over point, by increasing β for the first case and exactly opposite behavior is noticed for second case in which epilimnion layer (*i.e.* $S_t = 0$) is considered.

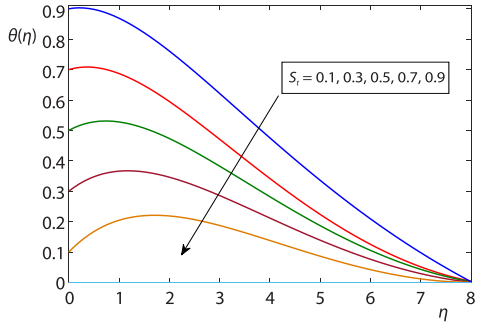

Figure 5. Temperature distribution for S_t

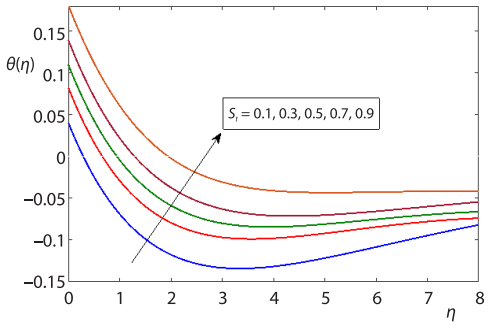

Figure 6. Temperature gradient for S_t

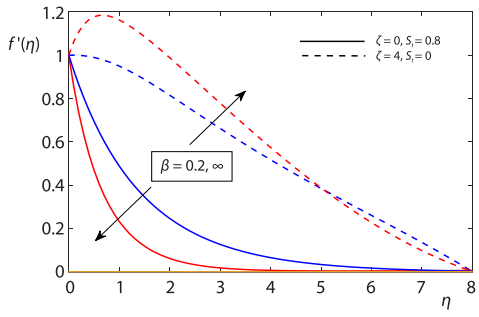

Figure 7. Velocity distribution for β

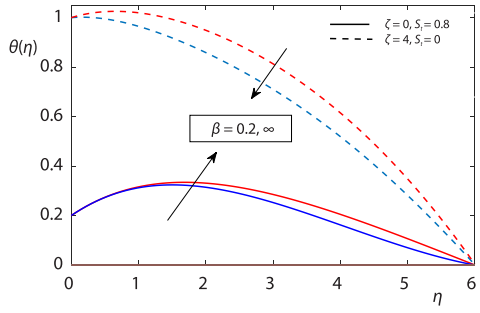

Figure 8. Temperature distribution for β

Figure 10 depicts the impact of parameter q_1 on $f'(\eta)$. In this figure both negative and positive values are considered. An increment is seen in $f'(\eta)$ for all negative and positive q_1. Figure 11 illustrates the impact of parameter q_1 on $\theta(\eta)$. An increment is seen in $\theta(\eta)$ for all negative and positive q_1. Figure 12 illustrates the impact of q_1 on $\theta'(\eta)$ profile. An increment is seen in $\theta'(\eta)$ alongside the surface for increased q_1, a crossover point is noticed between $2.1 < q_1 < 2.3$ after this temperature gradient decreases.

Figure 13 depicts the impact of parameter M on $f'(\eta)$. Two cases are considered for this study first is with stratification and second is without stratification. In both cases decreased velocity profile noticed for increased M. Reason for this decreasing pattern of velocity profile is that a Lorentz force is formed by a magnetic field created by the motion of an electrically conducted fluid, and it has the property of retardation. In the case when hypolimnion thermal stratification (*i.e.* $S_t = 0.8$) is considered this drag force become more effective and in epilimnion

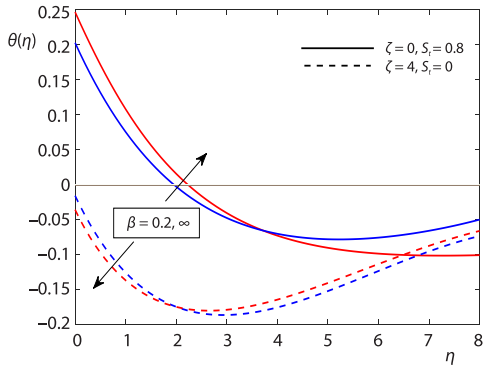

Figure 9. Temperature gradient distribution for β

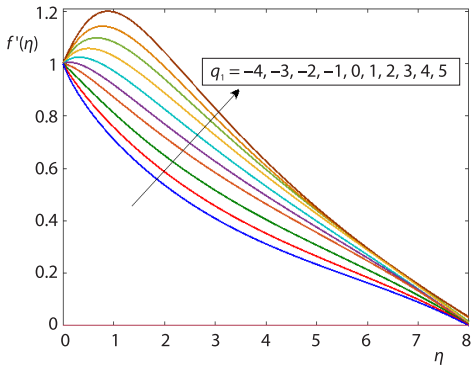

Figure 10. Velocity distribution for q_1

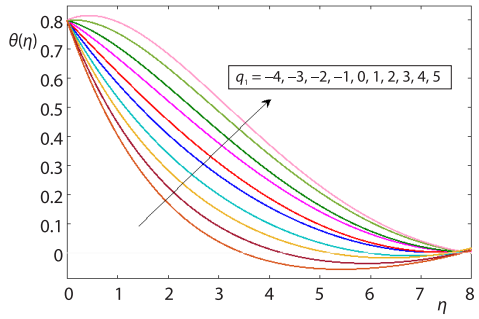

Figure 11. Temperature distribution for q_1

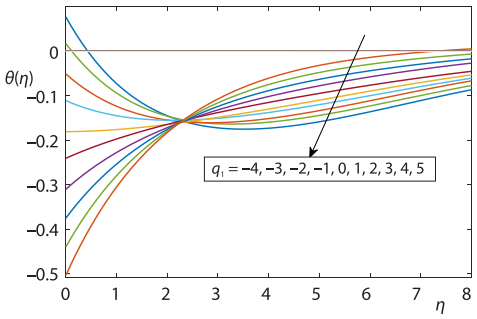

Figure 12. Temperature gradient distribution for q_1

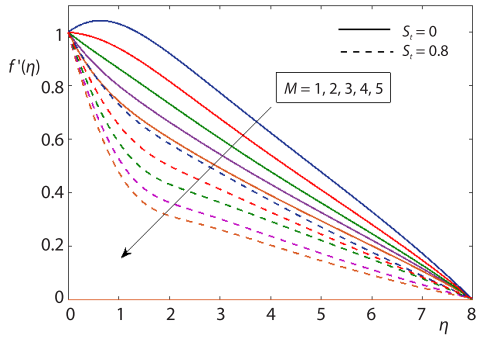

Figure 13. Velocity distribution for M

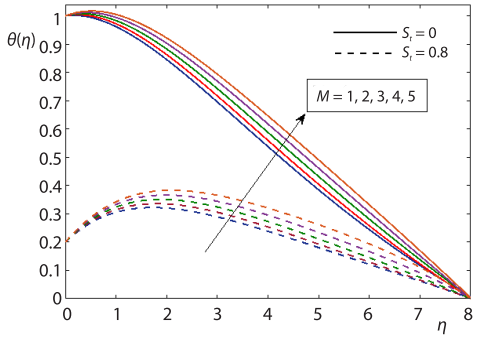

Figure 14. Temperature distribution for M

condition (*i.e.* $S_t = 0$) highest velocity is noticed. Both cases are depicted for temperature profile by fig. 14. With the fact that more heat produces with imposed magnetic field so an increased temperature profile is noticed with increasing M for both cases. In the case when hypolimnion thermal stratification (*i.e.* $S_t = 0.8$) is considered, parabolic profile with highest temperature is noticed and in epilimnion condition (*i.e.* $S_t = 0$) highest temperature is noticed near the wall. Figure 15 depicts the impact of parameter M on $\theta'(\eta)$. An increment is seen in $\theta'(\eta)$ near the wall for the values of M, a crossover point is noticed between $4.1 < M < 4.4$ after this temperature gradient decreases.

The impacts of K for $f'(\eta)$ is portrayed by fig. 16. It's been discovered that with decreased K a slowdown in $f'(\eta)$ is observed. With the fact $K \propto 1/k_0$ thus if porosity coefficient enhances, the medium's permeability decreases, this leads to lowering fluids velocity. Figures 17 and 18 depicts the impact of parameter K on $\theta(\eta)$ and $\theta'(\eta)$, respectively, with increased K temperature profile and temperature gradient increases significantly.

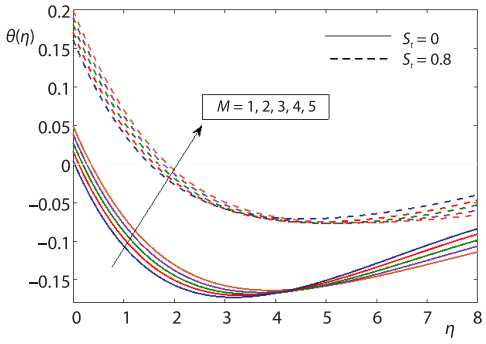

Figure 15. Temperature gradient distribution for *M*

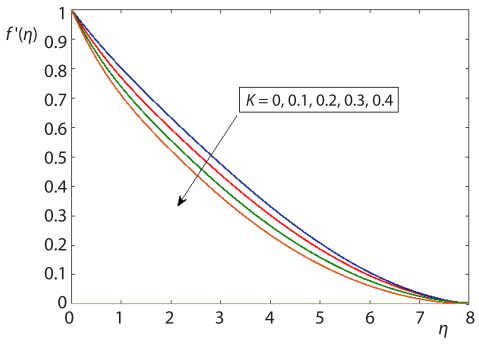

Figure 16. Velocity distribution for *K*

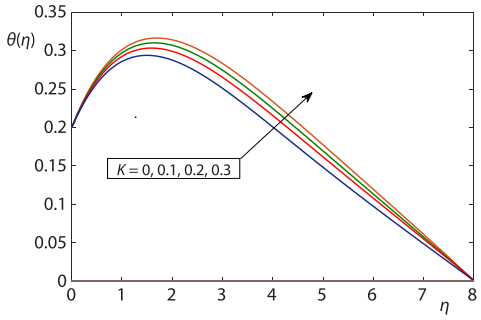

Figure 17. Temperature distribution for *K*

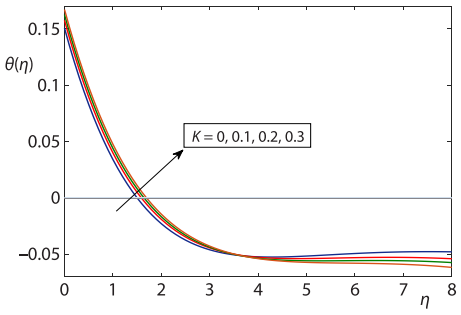

Figure 18. Temperature gradient distribution for *K*

Code verification

Comparisons with Animasaun [10], Bidin and Nazar [18], and Nadeem *et al.* [19] for local Nusselt numbers were done to validate this research, utilizing numerous values of Prandtl number as given in tab. 1. The other parameters in our mathematical model are considered zero to accomplish this ($\xi = \varepsilon = S_t = M = K = q_1 = \mathrm{Gr}_m = S = 0$ and $\beta = \infty$). The estimated results are found better agreement with previous results.

Table 1. Comparisons for several values of Prandtl number for $-\theta'(0)$, with radiation parameter *N*

$E = 0$ and $N = 0.5$ [18]	$\lambda_1 = \omega = B = E = 0$ [19]	$N = 0.5$ [10]	Present study, $N = 0.5$
0.6765	0.680	0.6796065524	0.6796065457
1.0735	1.073	1.0735232305	1.0735232409
1.3807	1.381	1.3807094061	1.3807094118

Conclusions

Casson fluids flow through an exponentially expanding sheet in permeable media is studied. This free convective MHD flow is investigated along with thermal stratification assuming viscosity and thermal conductivity, temperature dependent. Fourth ordered Runge-Kutta method considering shooting techniques is used to study the impact of various flow control parameters. Important results are as follows.

- With increased ξ an increasing velocity profile is noticed but a decrement is observed for $\theta(\eta)$ in entire domain and for $\theta'(\eta)$ near the wall.
- In this investigation it is concluded that with increased Casson fluids parameter decreasing velocity profile is noticed but an increment is observed for $\theta(\eta)$ in entire domain and for $\theta'(\eta)$ near the wall when fluid is considered with constant viscosity ($\xi = 0$ and $S_t = 8$) and reverse effect is noticed for the case when stratification is zero(*i.e.* $\xi = 4$ and $S_t = 0$).

References

[1] Crane, L. J., Flow Past a Stretching Plate, *Z Angew Math. Phys*., *21* (1970), 4, pp. 645-647
[2] Gupta, P. S., Gupta, A. S., Heat and Mass Transfer on a Stretching Sheet with Suction or Blowing, *The Canadian Journal of Chemical Engineering*, *55* (1977), 6, pp. 744-746
[3] Kumaran, V., Ramanaiah, G., A Note on the Flow over a Stretching Sheet, *Acta Mechanica*, *116* (1996), Mar., pp. 229-233
[4] Elbashbeshy, E. M. A., Heat Transfer over an Exponentially Stretching Continuous Surface with Suction, *Archives of Mechanics*, *53* (2001), 6, pp. 643-651
[5] Jat, R. N., *et al*., The MHD Boundary-Layer Flow and Heat Transfer of Caisson Fluid over a Moving Porous Plate with Viscous Dissipation and Thermal Radiation Effects, *Journal of Rajasthan Academy of Physical Sciences*, *16* (2017), 33-4, pp. 211-232
[6] Al-Odat, M. Q., *et al*., Thermal Boundary-Layer on an Exponentially Stretching Continuous Surface in the Presence of Magnetic Field Effect, *International Journal of Applied Mechanics and Engineering*, *11* (2006), 2, pp. 289-299
[7] Watanabe, T., Pop, I., Magnetohydrodynamic Free Convection Flow over a Wedge in the Presence of a Transverse Magnetic Field, *International Communications in Heat and Mass Transfer*, *20* (1993) 6, pp. 871-881
[8] Crepeau, J. C., Clarksean, R., Similarity Solutions of Natural-Convection with Internal Heat Generation, *Transactions of ASME – Journal of Heat Transfer*, *119* (1997), 1, pp. 184-185
[9] Dessie, H., Kishan, N., The MHD Effects on Heat Transfer over Stretching Sheet Embedded in Porous Medium with Variable Viscosity, Viscous Dissipation and Heat Source/Sink, *Ain Shams Engineering Journal*, 5 (2014), 3, pp. 967-977
[10] Animasaun, I. L., Casson Fluid-flow with Variable Viscosity and Thermal Conductivity along Exponentially Stretching Sheet Embedded in a Thermally Stratified Medium with Exponentially Heat Generation, *Journal of Heat and Mass Transfer Research*, *2* (2015), 2, pp. 63-78
[11] Mabood, F. *et al.*, Impact of Heat Generation/Absorption of Magnetohydrodynamics Oldroyd-B Fluid Impinging on an Inclined Stretching Sheet with Radiation, *Scientific Reports*, *10* (2020), 17688
[12] Tharapatla, G. *et al.*, Effects of Heat and Mass Transfer on MHD Non-Linear Free Convection Non-Newtonian Fluids Flow Embedded in a Thermally Stratified Porous Medium, *Heat Transfer*, *50* (2021), 4, pp. 3480- 3500
[13] Mukhopadhyay, S., Casson Fluid-Flow and Heat Transfer over a Non-Linearly Stretching Surface, *Chinese Physics*, *22* (2013), 7, 074701
[14] Abu-Romia, M. M., Pyare, R., Approximate Analysis for Transient Heat Conduction with Radiation in a Slab. *Appl. Sci. Res*., *24* (1971), Dec., pp. 354-366
[15] Abegunrin, O. A. *et al.*, Comparison between the Flow of Two Non-Newtonian Fluids over an Upper Horizontal Surface of Paraboloid of Revolution: Boundary-Layer Analysis, *Alexandria Engineering Journal*, *55* (2016), 3, pp. 1915-1929
[16] Agrawal, P. *et al.*, Magneto Marangoni flow of γ-AL_2O_3 Nanofluids with Thermal Radiation and Heat Source/Sink Effects over a Stretching Surface Embedded in Porous Medium*, Case Studies in Thermal Engineering*, *23* (2021), 100802

[17] Salem, A. M., Fathy, R., Effects of Variable Properties on MHD Heat and Mass Transfer Flow Near a Stagnation Point Towards a Stretching Sheet in a Porous Medium with Thermal Radiation, *Chinese Physics*, *B21* (2012), 5, pp. 1-11
[18] Bidin, B., Nazar, R., Numerical Solution of the Boundary-Layer Flow over an Exponentially Stretching Sheet with Thermal Radiation, *European Journal of Scientific Research, 33* (2009), Jan., pp. 710-717
[19] Nadeem, S. *et al.*, Effects of Thermal Radiation on the Boundary-Layer Flow of a Jeffrey Fluid over an Exponentially Stretching Surface, *Numerical Algorithms, 57* (2011), Sept., pp. 187-205

Paper submitted: February 11, 2022
Paper revised: March 14, 2022
Paper accepted: March 24, 2022